Heat Transfer Rate and Fluid Flow Analysis with Design Parameters of Gas Turbine using Beta-clog^2-LSTM

Mohammad Saraireh
Mechanical Engineering Department, Faculty of Engineering, Mutah University, Jordan
maqsaraireh@mutah.edu.jo (corresponding author)

Received: 16 June 2024 | Revised: 8 July 2024 | Accepted: 11 July 2024

 DOI: https://doi.org/10.48084/etasr.8152

ABSTRACT

A Gas Turbine (GT) is a combustion engine that converts fuel into mechanical energy. None of the conventional models has utilized the stator hub, rotor tip leakage, and inter-stage flow for the optimum design of GT. This study performs an effective design parameter analysis for GT with heat transfer rate and fluid flow detection using Betadecay with cloglog-based Long Short-Term Memory (Beta-clog^2-LSTM) and Griewank Siberian Tiger Optimization (G-STO). Initially, the design parameters were taken and the geometry of those parameters was created. Afterward, mesh generation was performed using the Linear Weighted Gradient Smoothing Sliding Mesh Interface (LWGSSMI). Then, the boundaries of the generated mesh were detected. Next, numeric modeling was performed deploying Finite Element Analysis (FEA), followed by flow behavior analysis. The optimal parameters were selected by G-STO. Similarly, the data in a heat transfer rate dataset were preprocessed and the features were extracted. Prediction of heat rate was performed using Beta-clog^2-LSTM. Finally, the thermal loss was calculated, and a heat exchanger was utilized to mitigate it. The performance analysis demonstrated the robustness of the proposed method by achieving 0.98 prediction accuracy.

Keywords-gas turbine; heat transfer rate; fluid flow; stator hub; rotor tip; power

I. INTRODUCTION

A Gas Turbine (GT) is an internal combustion engine that converts fuels, such as natural gas or fluids, to mechanical energy [1, 2]. This mechanical energy is then used to drive a generator to produce electrical energy and power machinery, such as an aircraft engine [3]. GT is widely emplloyed in power generation, aviation, and marine propulsion. GT operates in three phases: compression, combustion, and expansion. Fuel is first drawn into the GT through an inlet and then passed through a compressor. Compression aims to increase air pressure and make it more reactive with the fuel in the combustion stage [4]. Then, compressed air enters the combustion chamber, where fuel is also injected. In the chamber, the fuel is mixed with high-pressure air [5]. The fuel-air mixture is then ignited using some ignition sources. Combustion occurs by releasing a large amount of heat energy, which results in high-temperature and high-pressure combustion gases. Combustion aims to convert the chemical energy of the fuel into thermal energy in the form of hot and high-pressure gases [6]. A high temperature or heat is produced as an outcome of the combustion of fuel in the presence of compressed air. Thus, transferring the heat generated is an essential step in enhancing the GT durability. Furthermore, managing the heat generated in GT is crucial for efficient and safe operation [7]. High-pressure gases expand rapidly as they exit the combustion chamber [8]. These gases flow through the turbine, which consists of multiple stages of blades and vanes mounted on a shaft [9]. The expansion of gases drives the turbine blades, which in turn convert thermal energy into mechanical energy [10]. Mechanical energy from the rotating turbine shaft is used to drive GT in a closed loop and other machinery, such as an electrical generator or a propulsion system in an aircraft [11]. After passing through the turbine, the exhausted gases lose their energy due to work on the turbine blades and are expelled through an exhaust outlet [12]. In combined-cycle power plants, these exhaust gases can be utilized to produce steam for additional power generation, which improves the overall efficiency of the GT [13].

In GT, flow irreversibility is an inherent loss that occurs during energy conversion and prevents complete recovery of the input energy [14]. Therefore, analyzing and mitigating fluid flow issues is essential. In [15], a model was developed to analyze the flow irreversibility and heat transfer effects on turbine efficiency. Aerodynamic and aerothermal efficiency expressions were employed to assess the shaft power with the heat transfer effect. The experimental analysis showed that this model was effectively used to develop reduced-order fluid machinery models. However, this model had thermal losses. A Computational Fluid Dynamics (CFD) simulation model was introduced to analyze the activating processes of the rotor dynamics of a horizontal axis wind turbine [16]. The momentum analysis theory and the blade element momentum

model were deployed to predict the power generation rate. The evaluation findings exhibited that this model achieved better results, even in the low wind speed range. However, this model was inefficient during unsteady flow behavior.

In [17], a small-scale single-stage axial flow turbine model was presented for organic Rankine cycle application. Turbine pressure ratios and working fluids were analyzed through energy analysis and optimization with low computational intensity. The analysis showed that this model effectively enhanced the overall loss coefficient of the turbine. However, this model did not accurately predict the heat transfer rate. A non-axisymmetric end wall with non-axisymmetric contouring and GT purge flow was demonstrated in [18]. This model utilized aerodynamic loss, film cooling effectiveness, and the heat transfer coefficient as the objective function for aero-thermal optimization. The experimental results stated that this model significantly reduced the aerodynamic loss of GT. However, this model had increased the thermal load of the rear part on the end wall. In [19], a data-driven model was implemented for the conjugate heat transfer analysis of a GT vane. In this model, an experimental database of film cooling units was employed under multiple parameters to analyze the heat transfers of GT. The evaluation results revealed that this model achieved high heat rate prediction accuracy. However, it was time-consuming due to the utilization of a complicated cooling structure.

In [20], a high-temperature rotor blade model of a heavy GT was presented to analyze the rotation effect on flow and heat transfer [20]. The composite inner cooling structures of the rotor blades were modeled by coupling heat transfer simulation. The analysis disclosed that this model had increased the slope of the limiting streamline, which had a decisive influence on the heat transfer rate. However, the complexity of the model was high due to the detection of flow and heat transfer in the rotation state. In [21], a Bayesian model was introduced to analyze the 2D inverse heat transfer problem of GT discs, estimating both the upstream and downstream disc surfaces. A maternal covariance matrix was employed with the Gaussian prior distribution to evaluate the Bayesian model. The results manifested that the model had robust performance in detecting the problem of inverse heat transfer with better accuracy. However, data quality affected Bayesian results. In [23], a topology of the vortex structure and heat transfer analysis was employed on the internal tip of the GT blades. Delta-Winglet Vortex Generators (DWVG) were arranged at multiple tip locations to analyze the common-flow-up and common-flow-down configurations. The results showed that the common-flow-down configuration significantly enhanced the heat transfer rate. However, this model had slower execution due to the limited capacity of the heat transfer structure.

In [23], the internal surface of the tip wall was developed with a DWVG for the flow behavior and heat transfer rate analysis of GT blades. A smooth internal cooling channel was considered as the baseline and the fluid flow was identified by topological analysis in the skin friction field. The evaluation results exhibited that this model robustly achieved better heat transfer augmentation. However, adjusting the leading edge spacing in DWVG significantly affected the heat transfer performance. In [24], a hydrogen-fueled GT model was presented for the precool and intercool analysis of a compression system, integrated with heat management concepts using Liquid-Hydrogen2. Brayton cycle-based turbofans and staggered tube compact heat exchangers were deployed in this model. The experimental evaluation of this model demonstrated that specific fuel consumption was improved, enhancing the effectiveness of the heat exchanger. However, the reduction in the Mach number of the external airflow led to pressure dropout in the heat exchanger.

Several studies analyzed the heat transfer rate and fluid flow in GTs using CFD, FEA, Conjugate Heat Transfer (CHT), heat balance methods, thermodynamic cycle analysis, Multi-Disciplinary Optimization (MDO), and various Machine Learning (ML) and Deep Learning (DL) models [25, 26]. However, these models had some thermal losses, which in turn reduced the GT's efficiency. The current study proposes an effective heat transfer rate and fluid flow analysis on GT design parameters using Beta-clog^2-LSTM and G-STO.

A. Problem Statement

- A multi-stage optimum design for a typical cycle gas turbine, considering the stator hub, rotor tip leakage, and inter-stage flow, was not investigated in any previous study.
- The adiabatic process in [15] was free from aerodynamic losses. However, it was not free from thermal losses, which degraded the potential efficiency of the turbine.
- The heat transfer rate in [17] was not accurately predicted, which was the key factor in designing the cooling system, as the wall absorbed some heat from the flow of the fluids.
- Due to the non-fully irreversible process of the flow across the mixing plane, errors might have occured in previous studies.
- The conventional Moving Reference Frame (MRF) method in [16] was inefficient during unsteady flow and blade-vortex interactions that took place at a high tip speed ratio.

B. Objectives

- Effectively employ optimal designs of stator hub, rotor, and inter-stage.
- Detect the thermal losses by EPC-FLS.
- Accurately predict the heat transfer rate using Beta-clog^2-LSTM.
- Reduce the error across the mixing plane by calculating the shear stress in CFD and FEA.
- Accurately capture the unsteady flow by the proposed LWGSSMI.

II. METHODOLOGY

The heat transfer rate and fluid flow of the GT were analyzed using Beta-clog^2-LSTM and G-STO methods. The design parameters for the stator hub, rotor, and inter-stage were analyzed and optimized utilizing G-STO. Subsequently, the

heat rate prediction was performed deploying Beta-clog^2-LSTM. Figure 1 shows the architecture of the proposed framework.

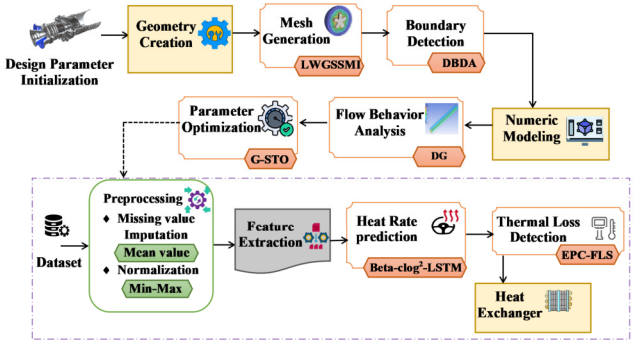

Fig. 1. Architecture of the proposed framework.

A. Design Parameter Initialization

Initially, the design parameters of the stator hub, rotor, and inter-stage are defined. The design parameters of the stator hub (Ω) are the stator blade numbers, blade angle, and blade profile. For the rotor (δ), the design parameters are the blade profiles, lean stacking line, twist stacking line, and rotor blade numbers. Also, the parameters used for designing inter-stage (α) are the geometry of the inter-stage passage and the sealing between stages. Thus, the total design parameters (ϑ) used to design the GT are described as:

$$\vartheta = \{\Omega \oplus \delta \oplus \alpha\} \quad (1)$$

Then, based on ϑ, the GT is further designed by analyzing and optimizing the parameters. Afterwards, the parameters are inputted into the CFD simulation.

B. CFD Simulation

The CFD simulation is implemented to generate the GT model with ϑ to analyze the fluid flow process by creating geometry models, mesh generation, and boundary detection. The CFD simulation process is described as follows.

1) Geometry creation

This is a process to define and develop the three-dimensional shapes and configurations of ϑ. Geometry creation describes the control sections and blade stacking line in ϑ. The created geometry of ϑ is denoted as ϑ^{geo}.

2) Mesh Generation

Afterwards, the mesh of ϑ^{geo} is generated using LWGSSMI. The conventional Sliding Mesh Interface (SMI) captures the intricate interaction between the stationary and rotating parts in a turbine. The complex interaction information helps to understand the pressure fluctuations, boundary layer effects, and flow separation around blades or vanes in the turbine. However, the distorted mesh in SMI can produce inaccurate outcomes. To overcome this issue, a linear weighted gradient smoothing function is employed. At first, the LWGSSMI process decomposes the computational domain of ϑ^{geo} into stationary and rotating parts. Then, the fluid's flow through ϑ^{geo} is governed by the Navier-Stokes equation as in [27].

$$\hat{\mu} \cdot \frac{\partial u}{\partial t} + (u \cdot \nabla)u = \frac{1}{\rho}\nabla p + \nu\nabla^2 u + f \quad (2)$$

where u denotes the velocity vector, ρ is the fluid density, p and ν represent the pressure and kinematic viscosity, respectively, t denotes time, f represents the body force of ϑ^{geo}, and $\hat{\mu}$ denotes the linear weighted gradient smoothing function. Then, the mesh is generated as stationary (stator mesh), rotating (rotor mesh), and interface mesh between the stator and rotor.

3) Boundary Detection

Then, the boundary of Ξ is determined using the Deep Boundary Detection Algorithm (DBDA). DBDA can effectively detect the edges or boundaries within a distributed system. The boundary of Ξ is detected based on the following steps:

1. Initially, the nodes, which are the slides of Ξ, are initialized with their own data (υ) and position (g) information. Thus, the data value is represented as υ_g.
2. The nodes communicate with the neighbor nodes (ς) to share the local data.
3. Each node performs local computation to detect if the node is lying on a boundary by using gradient calculation and thresholding process. The gradient (∇) is computed to determine the changes in υ_g as in [28].

$$\nabla\upsilon_g = \left(\frac{\partial\upsilon}{\partial X}\Big|_g, \frac{\partial\upsilon}{\partial Y}\Big|_g\right) \quad (3)$$

where X and Y indicate the axis of the gradient. Then, the magnitude of the gradient $(\|\nabla\upsilon_g\|)$ is compared with the threshold (Γ), represented as in [28].

$$\|\nabla\upsilon_g\| = \sqrt{\left(\frac{\partial\upsilon}{\partial X}\Big|_g\right)^2 + \left(\frac{\partial\upsilon}{\partial Y}\Big|_g\right)^2} \quad (4)$$

$$\psi = \begin{cases} if(\|\nabla\upsilon_g\| > \Gamma), then\ \psi \\ else, otherwise \end{cases} \quad (5)$$

where ψ indicates the boundary.

4. The boundary nodes collaborate to refine the detected boundaries by exchanging boundary information to achieve the global consensus, illustrated as:

$$\Omega_g^{l+1} = \frac{1}{\varsigma_g + 1}\left(\Omega_g^l + \sum_{G\in\varsigma}\Omega_G^l\right) \quad (6)$$

where Ω denotes the boundary status, l denotes the iteration, and G denotes one neighbor node.

5. Finally, each node reports the Ω to the aggregation node. Thus, using the above process, the boundary of the generated Ξ is detected. Hence, the CFD simulation model (υ) is effectively designed.

C. Numerical Modeling

Subsequently, υ is numerically verified utilizing FEA based on Ξ and ψ. The partial differential equation is employed to define the modeling problem. Then, the domain is divided into subdomains called finite elements. Then, the stiffness matrix and load vector of Ξ are estimated. The boundary conditions from ψ are applied to enforce the known forces of GT. Finally, the shear stress (τ) is calculated to minimize the error in the GT design, defined as in [27].

$$\tau = \mu \frac{du}{dy} \tag{7}$$

where y denotes the distance, and μ is the dynamic viscosity. Then, the flow behavior of the fluids in the error-minimized GT design (e) is further analyzed.

D. Flow Behavior

The flow behavior (Π) of e is analyzed using the Directed Graph (DG). The DG is also known as a digraph in which the edges of the graph are represented with an arrow indicating the direction of one vertex to another. The DG is described as:

$$\Pi = (\zeta', \phi)_e \tag{8}$$

where ζ' and ϕ indicate the number of nodes and edges in e, respectively. Thus, the flow behavior of the fluid is effectively attained from DG.

E. Parameter Optimization

The parameters υ and Π are optimized using G-STO and combined, indicated as $\wp$. The traditional Siberian Tiger Optimization (STO) incorporates two phases that mimic the hunting behavior of Siberian tigers. STO is deployed to optimize the design parameters because it provides an effective balance between the exploration and exploitation phases. However, STO gets stuck in local optima, so it might not give better solutions. To mitigate this problem, the Griewank function is used in the exploration phase. Let, the input for G-STO be $\wp$, which is described as the population of Siberian tigers. The process of G-STO is described as follows:

1. Initialization: At first, the population of the Siberian tigers is initialized as:

$$\wp = \{\wp_1, \wp_2, \ldots\ldots\ldots, \wp_s\} \tag{9}$$

where $\wp$ denotes the number of Siberian tigers in the population. Then, the initial position (P) of the Siberian tiger in the search place (d) is determined as in [29].

$$P_a^{b,d} = l^d + \varepsilon \times (u^d - l^d) \tag{10}$$

where $P_a^{b,d}$ denotes the b^{th} position of the a^{th} Siberian tiger in d, ε represents the random number, and u^d and l^d denote the upper and lower boundaries of d. The fitness (γ) of the Siberian tigers is determined as the minimum (min) systematic error $(\hbar)$ and gross error (ge), as:

$$\gamma = \min_{\wp_s}\{\hbar, ge\} \tag{11}$$

2. Prey hunting: The position of the Siberian tiger changes to hunt the prey. Based on γ, the position of the Siberian tiger is updated in the first exploration phase to attack the prey as:

$$P_{a,1}^{b,d} = P_a^{b,d} + \varepsilon \cdot \left(S - \varepsilon \cdot P_a^{b,d}\right) \tag{12}$$

where $P_{a,1}^{b,d}$ denotes the new position of the Siberian tiger in the first phase and S represents one Siberian tiger. This new position is updated only after analyzing the fitness of the Siberian tiger in that new position, and it is described as:

$$P_a^{b,d} = \begin{cases} P_{a,1}^{b,d}, if \gamma\left(P_{a,1}^{b,d}\right) > \gamma\left(P_a^{b,d}\right) \\ P_a^{b,d}, else \end{cases} \tag{13}$$

where $\gamma\left(P_{a,1}^{b,d}\right)$ and $\gamma\left(P_a^{b,d}\right)$ denote the fitness of the Siberian tiger in the new and old positions, respectively. Next, based on the chase process to hunt the prey, a new position for the Siberian tiger is estimated as:

$$P_{a,2}^{b,d} = P_a^{b,d} + \frac{\varepsilon \cdot (u^d - l^d)}{T} \tag{14}$$

where $P_{a,2}^{b,d}$ denotes the new position of the Siberian tiger in the second phase and T denotes the number of iterations.

3. Fighting with bear: Based on the attack and conflict between the bear and the Siberian tiger, the exploitation phase is categorized into two stages. In stage 1, one member from the population is selected by using the Griewank function [30], described as:

$$K = \frac{1}{4000}\sum_{i=1}^{d} K_i^2 - \prod_{i=1}^{d} cos\left(\frac{K_i}{\sqrt{i}}\right) + 1 \tag{15}$$

where i denotes the position of the K^{th} member in d. Then, the new position of the Siberian tiger in the first stage of the exploitation phase is generated as:

$$\tilde{P}_{a,1}^{b,d} = P_a^{b,d} + \varepsilon \cdot \left(K_a^{b,d} - \varepsilon \cdot P_a^{b,d}\right) \tag{16}$$

where $\tilde{P}_{a,1}^{b,d}$ is the new position of the Siberian tiger and $K_a^{b,d}$ denotes the position of the selected population member.

The above process continues until the maximum iteration is reached. Finally, the candidate's best solution is obtained, which is the optimal parameter $\left(\wp_{opt}\right)$.

ALGORITHM 1: PSEUDO-CODE FOR G-STO

```
Input: Parameters (℘)
Output: Optimal parameters(℘_opt)

Begin
Initialize Population (℘), γ, iteration (T), d, and
upper (u) and lower (l) bounds
For each ℘ do
  Initialize position
  Formulate γ = min_{℘_s}{ħ, ge}
  # Hunting prey phase
  Calculate new position based on φ,
  P_{a,1}^{b,d} = P_a^{b,d} + ε · (S − ε · P_a^{b,d})
  Update new position
  Evaluate new position based on chase process,
  P_{a,2}^{b,d} = P_a^{b,d} + ε·(u^d − l^d)/T
  Update new position
  #Fighting with bear phase
```

```
    Estimate new position based on bear's location,
    P̃^{b,d}_{a,1} = P^{b,d}_a + ε · (K^{b,d}_a − ε · P^{b,d}_a)
    Update new position
    Compute new position based on simulation of the
    conflicts,
    P̃^{b,d}_{a,2} = P^{b,d}_a + (ε/T) · (u^d − l^d)
    Update new position
End For
Return Optimal parameters
End
```

F. Thermal Loss Prediction

The thermal loss is calculated using the data from the heat transfer dataset. Then, the heat rate is predicted first and the thermal losses in the heat rate are detected followed by the proper heat exchanger to mitigate the loss.

1) Preprocessing

Initially, the c number of data (ℓ) is collected from the heat transfer rate dataset, described as:

$$\ell = \{\ell_1, \ell_2, \ldots\ldots, \ell_c\} \quad (17)$$

Thereafter, ℓ is preprocessed using the missing value imputation and normalization processes.

a) Missing Value Imputation

The missing values in ℓ are imputed deploying the mean value technique. The mean (ℓ^{mean}) of ℓ is taken and imputed to the missing place in ℓ, described as:

$$\ell^{mean} = \frac{\ell^{sum}}{\ell^{tot}} \quad (18)$$

where ℓ^{sum} and ℓ^{tot} denote the sum of ℓ and total number of data in ℓ, respectively. Thus, the obtained ℓ^{mean} replaces the missing values in ℓ, and the missing value imputed data is represented as ℓ^{mis}.

b) Normalization

The normalization of ℓ^{mis} is performed employing the min-max normalization technique, described as:

$$\varpi = \frac{\ell^{mis} - min(\ell^{mis})}{max(\ell^{mis}) - min(\ell^{mis})} \quad (19)$$

where min and max denote the minimum and maximum values, respectively, and ϖ represents the normalized data.

2) Feature Extraction

From ϖ, the features of the heat transfer coefficient of the fluid, Nusselt number for the fluid side, thermal conductivity, heat capacity ratio, mass flow rate of the cold fluid, mass flow rate of the hot fluid, heat transfer rate, heat transfer rate of the fluid, total heat transfer rate, heat transfer area for the fluid side, total heat transfer area, heat transfer area for the bulk side, mass flow rate of the fluid, relative change in heat transfer rate, change in heat transfer rate per unit mass flow rate, heat transfer coefficient for the shell side, fin efficiency, exact efficiency, nominal efficiency, and overall heat transfer resistance are extracted to train the proposed heat rate prediction system. The extracted features are represented as $\bar{\lambda}$.

3) Heat Rate Prediction

Based on $\bar{\lambda}$, the heat rate is predicted using the Beta-clog^2-LSTM. The traditional LSTM has a specific architecture with gated mechanisms that control information flow, mitigating vanishing gradient problems and allowing them to learn from longer sequences. However, LSTMs are susceptible to overfitting, especially with insufficient data. To overcome the issue, the Beta decay regularization method and the cloglog activation function are employed. Figure 2 depicts the structure of the Beta-clog^2-LSTM.

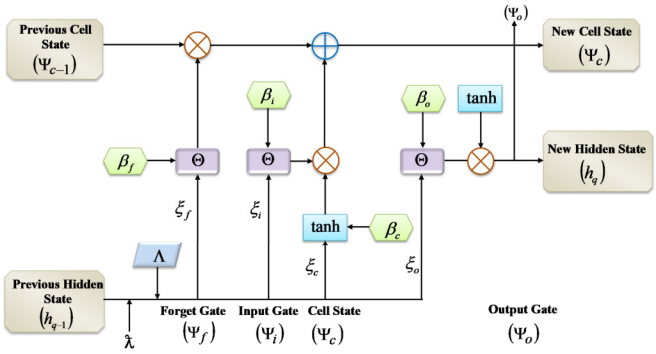

Fig. 2. Structure of the proposed Beta-clog^2-LSTM.

1. Forget gate: The unused information in the previous cell state is removed by the forget gate (Ψ_f). Ψ_f determines which data should passed through the cell by:

$$\Psi_f = \Lambda\Theta \cdot \left(\xi_f \cdot \left[h_{q-1}, \bar{\lambda}\right] + \beta_f\right) \quad (20)$$

where Λ denotes the beta decay regularization, h_{q-1} denotes the previous hidden state, ξ_f denotes the weight factor, β_f represents the bias factor, and Θ denotes the cloglog activation.

2. Input gate: The input gate (Ψ_i) controls the information that flows into the cell state (Ψ_c), described as:

$$\Psi_i = \Theta \cdot \tilde{\Gamma}_c\left(\xi_i \cdot \left[h_{q-1}, \bar{\lambda}\right] + \beta_i\right) \quad (21)$$

where ξ_i *and* β_i denote the bias and weight factors of the input gate, respectively, and $\tilde{\Psi}_c$ denotes the vector function of Ψ_c.

3. Cell state: Ψ_c is considered as the network memory to store the data. $\tilde{\Psi}_c$ and Ψ_c are represented as:

$$\tilde{\Psi}_c = tanh \cdot \left(\xi_c \cdot \left[h_{q-1}, \bar{\lambda}\right] + \beta_c\right) \quad (22)$$

$$\Psi_c = \Psi_f \circ \Psi_{c-1} + \Psi_i \circ \tilde{\Psi}_c \quad (23)$$

where Ψ_{c-1} denotes the previous cell state and ξ_c and β_c are the weight and bias terms of Ψ_c, respectively.

4. Output gate: The output gate (Ψ_o) regulates the information in Ψ_c and generates the next hidden state (h_q).

$$\Psi_o = \Theta \cdot \left(\xi_o \cdot \left[h_{q-1}, \bar{\lambda}\right] + \beta_o\right) \quad (24)$$

$$h_t = \Psi_o \cdot tanh(\Psi_c) \quad (25)$$

where h_q denotes the next hidden state, ξ_o denotes the weight factor of Ψ_o, and β_o represents the bias factor of Ψ_o. Then, the loss function(ι) is determined to estimate the reliability of the Beta-clog^2-LSTM. Thus, Ψ_o is obtained with the heat rate (q). Algorithm 2 shows the pseudo-code for Beta-clog^2-LSTM.

ALGORITHM 2: PSEUDO-CODE FOR BETA-CLOG^2-LSTM

```
Input: Extracted features (λ̃)
Output: Heat rate (q)

Begin
Initialize bias factor (β) and weight factor (ξ)
For each λ̃ do
  Estimate forget gate function
  Activate Θ = 1 − e^{−e'(λ)}
  Formulate Λ = log(Σ_{λ=1}^{ς'} e^{'α_λ}) = SM(α̂_λ)
  Compute input gate function,
  Ψ_i = Θ · Γ̃_c(ξ_i · [h_{q−1}, λ̃] + β_i)
  Evaluate Ψ_c = Ψ_f ∘ Ψ_{c−1} + Ψ_i ∘ Ψ̂_c
  Process output gate
  Generate next hidden state,
  h_t = Ψ_o · tanh(Ψ_c)
  Determine ι
  If (ι = satisfied){
    Terminate
  }
  else {
    Tune the parameters
  }
  End If
End For
Return Heat rate
End
```

G. Thermal Loss Detection

The thermal loss in q is detected using EPC-FLS. Fuzzy Logic Systems (FLS) are less susceptible to noise or errors in the input data compared to crisp logic systems. Even with slight variations in the inputs, the fuzzy system can still provide a reasonable output. This makes them robust and adaptable to real-world conditions, where data may not always be perfectly accurate. However, the specific output reached by the FLS system is complex because of the interplay of multiple fuzzy rules and membership functions. The exponential polyhedral conic membership function is applied to overcome this drawback. At first, the condition for identifying the thermal loss is determined as:

$$J = \begin{cases} if\left(q = \wp_{opt}\right), then\ 0 \\ else, then\ 1 \end{cases} \quad (26)$$

where 0 and 1 indicate the absence and presence of thermal loss, respectively. Afterwards, the fuzzification block $(\Re)$ of EPC-FLS maps the input (J) into a fuzzy value (J') using:

$$J \xrightarrow{\Re} J' \quad (27)$$

Then J' is forwarded to the inference engine, and it is responsible for decision-making based on EPC-FLS using the exponential polyhedral conic membership function given as:

$$\Phi = exp(o * [\Delta * J' - u]) \quad (28)$$

where o and u describe the scaling parameter and threshold vector, respectively, Δ represents the coefficient matrix, and exp indicates the standard exponential function. Finally, the fuzzy value from Φ is transformed into the original crisp input (J) in the defuzzification block $(\Im)$, represented as:

$$\Phi \xrightarrow{\Im} J \quad (29)$$

The presence or absence of thermal loss is estimated from J. Finally, the heat exchanger $(\aleph)$is used to mitigate the thermal loss based on:

$$\kappa = \begin{cases} J = 1, then\ \aleph \\ J = 0, otherwise \end{cases} \quad (30)$$

where 1 and 0 indicate the presence and absence of thermal loss, respectively.

III. RESULTS AND DISCUSSION

The efficacy of the proposed model was compared with existing models. The proposed model was implemented in MATLAB.

A. Dataset Description

The heat transfer dataset was implemented to train and evaluate the reliability of the proposed model. The dataset [31] consists of 100 heat transfer rate data of the turbines. Among all data, 80% are used to train the proposed system, and the remaining 20% are used to test its efficiency.

B. Performance Analysis

The performance of the proposed method was analyzed and compared with those of the existing models. Figure 3 portrays the power output and the efficiency of the proposed model.

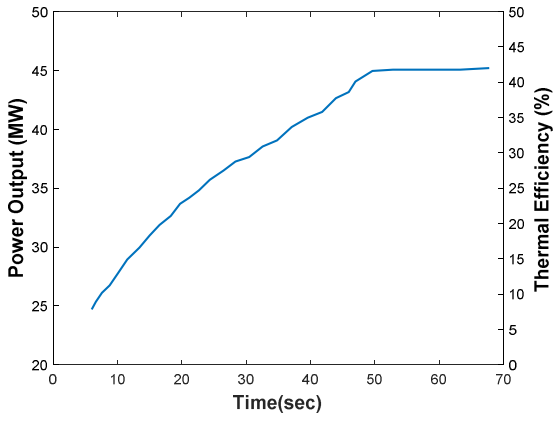

Fig. 3. Power and efficiency analysis of the proposed model.

Figure 3 exhibits the whole power output from the designed GT and the efficiency rate of the proposed model. The output power from the proposed model is 48.65 MW and the efficiency rate is 42.9%. These results were achieved by effective heat transfer rate prediction and mitigation of the thermal losses occurring on the heat rate of the GT using Beta-clog^2-LSTM and EPC-FLS, respectively.

1) Performance Evaluation of the Proposed Beta-clog^2-LSTM

The efficiency of the proposed Beta-clog^2-LSTM was compared with that of existing models, such as Long Short-Term Memory (LSTM), Deep Neural Network (DNN), Convolutional Neural Network (CNN), and Artificial Neural Network (ANN).

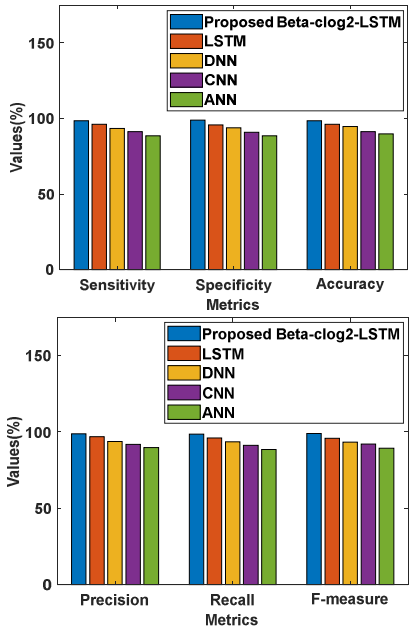

Fig. 4. Performance evaluation of the proposed Beta-clog^2-LSTM method based on (a) sensitivity, specificity, and accuracy and (b) precision, recall, and F-measure.

The proposed model effectively reduced the overfitting issue in the conventional model by employing the cloglog activation function. The proposed Beta-clog^2-LSTM achieved 98.56% sensitivity, 98.91% specificity, 98.55% accuracy, 98.9% precision, 98.56% recall, and 99.01% f-measure values. The other existing models had significantly lower performance measures, proving the robustness of the proposed model.

TABLE I. FPR AND FNR ANALYSIS

Technique	FPR	FNR
Proposed-Beta-clog^2-LSTM	0.007185	0.00678
LSTM	0.009292	0.00815
DNN	0.01463	0.01348
CNN	0.01894	0.01812
ANN	0.02577	0.02678

TABLE II. NPV AND MCC ASSESSMENT

Methods	NPV	MCC
Proposed-Beta-clog^2-LSTM	0.9841	0.9879
LSTM	0.9581	0.9683
DNN	0.9286	0.9361
CNN	0.9156	0.9058
ANN	0.8867	0.8931

Tables I and II illustrate the False Positive Rate (FPR), False Negative Rate (FNR), Negative Predictive Value (NPV), and Matthews Correlation Coefficient (MCC) analysis of the proposed Beta-clog^2-LSTM and existing models. The FPR, FNR, NPV, and MCC of the exiting LSTM were 0.009292, 0.00815, 0.9581, and 0.9683, respectively. However, the proposed model had FPR, FNR, NPV, and MCC of 0.007185, 0.00678, 0.9841, and 0.9879, respectively. This robust performance is achieved using the beta decay regularization method, showing that the proposed model is less error-prone.

2) Performance Assessment of the Proposed EPC-FLS

The performance of the proposed EPC-FLS and that of other existing models, such as Triangular FLS, FLS, Adaptive Neuro-fuzzy Inference System (ANFIS), and Decision rule were also evaluated, as evidenced in Figure 5.

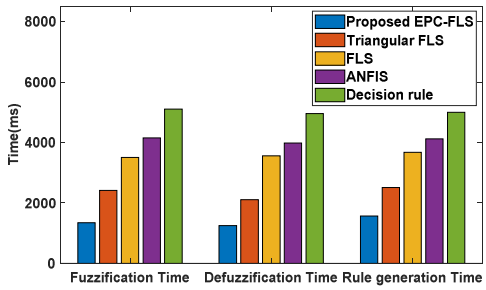

Fig. 5. Performance of the proposed EPC-FLS.

The performance of the proposed was better than that of the existing models, as the proposed EPC-FLS reduced the complexity of the conventional model by using the exponential polyhedral conic membership function. Thus, the proposed model took a minimum time of 1345 ms, 1247 ms, and 1568 ms for fuzzification, defuzzification, and rule generation, respectively. Decision rule took 5111 ms, 4960 ms, and 4999 ms time for fuzzification, defuzzification, and rule generation, which are considerably longer than the minimum time taken by the proposed model.

3) Performance Analysis of the Proposed G-STO

The performance of the proposed G-STO was analyzed and compared with that of traditional models, such as STO, Sea Horse Optimization (SHO), Ant Colony Optimization (ACO), and Scalp Swarm Optimization (SSO). Figure 6 shows a fitness vs. iteration analysis. The proposed G-STO dynamically overcame the local optima solution problem in the conventional STO model and achieved minimum systematic and gross error values. For 20 iterations, the fitness of the proposed G-STO was 0.21245, while the existing SSO had 0.3451. For 50 iterations, the fitness of the proposed and existing SSO models was 0.123 and 0.26456, respectively. The other models achieved higher error values than those of the proposed model. Thus, the fitness of the proposed model was more effective.

C. Comparative Analysis with Related Works

A comparative analysis of the proposed model and previous studies was carried out on the heat transfer rate and fluid flow analysis of a GT.

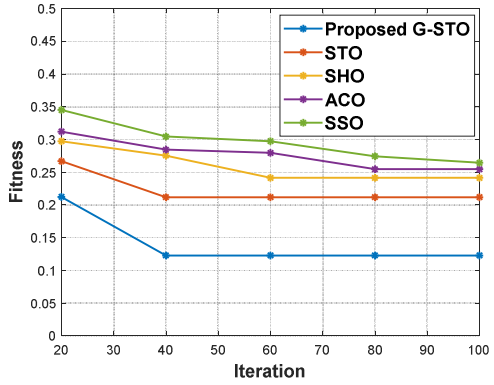

Fig. 6. Fitness vs. iteration analysis.

TABLE III. COMPARATIVE ANALYSIS WITH RELATED WORKS

Ref.	Objective	Methodology	Power (MW)	Efficiency (%)
Proposed	Heat transfer and fluid flow analysis of GT	Beta-clog^2-LSTM	48.65	42.9
[32]	Dynamic simulation of GT for heat recovery	Graphical modular modeling	11.35	-
[33]	Heat Transfer intensification in radial channels of GT blades	Asymmetric method	-	33
[34]	Performance optimization and exergy analysis of thermoelectric heat recovery system for GT	Thermoelectric system	10.5	-
[35]	Optimal structure design of supercritical carbon dioxide power cycle for GT waste heat recovery	Super-structure optimization model	46.36	21.47
[36]	Finite physical dimensions thermodynamics analysis and design of closed irreversible cycles for GT	Finite physical dimensions thermodynamics	-	35

Table III provides a comparative analysis of the proposed and related works. Previous works utilized several methods, such as graphical modular modeling, asymmetric method, thermoelectric system, super-structure optimization model, and finite physical dimensions thermodynamics to analyze the efficiency of GT. The proposed model effectively overcame the limitations of traditional models with 48.65 MW power output and 42.9% efficiency. Other models, such as those presented in [32] and [33], had only 11.35 MW power and 33% efficiency, respectively. Similarly, the other models also attained lower output power and efficiency than the introduced one.

IV. CONCLUSIONS

This study proposed a significant GT modeling framework based on design parameter optimization along with heat transfer rate identification and fluid flow effect analysis. The reliability of the proposed model was proven by implementing it in MATLAB. The experimental analysis revealed that the proposed Beta-clog^2-LSTM model achieved 98.55% and 99.01% detection accuracy and f-measure, respectively. The proposed EPC-FLS takes a minimum time of 1345 ms, 1247 ms, and 1568 ms for the fuzzification, defuzzification, and rule generation of thermal loss detection, respectively. The fitness of the proposed G-STO was also better than that of existing models, showing that it is less error-prone. The overall analysis proved the robustness of the proposed model in designing a GT model with minimum error and maximum efficiency. The proposed model designed a GT model by optimizing the parameters and also predicting the heat rate and thermal losses. In the future, the efficiency of the model introduced will be improved by analyzing the turbine's fuel mass flow and rotation speed to realize the power balance using 3D CFD.

REFERENCES

[1] A. Farooq, S. Hussain, X. Li, and M. A. Khan, "Fluid flow characteristics and convective heat transfer improvement on a gas turbine blade," *Heat Transfer*, vol. 50, no. 8, pp. 8403–8425, 2021, https://doi.org/10.1002/htj.22282.

[2] S. Stratila, D. Glasberg, and I. Mălăel, "Performance Analysis of a New Vertical Axis Turbine Design for Household Usage," *Engineering, Technology & Applied Science Research*, vol. 14, no. 1, pp. 12536–12542, Feb. 2024, https://doi.org/10.48084/etasr.6559.

[3] M. A. Khader, M. Ghavami, J. Al-Zaili, and A. I. Sayma, "Heat Transfer Effect on Micro Gas Turbine Performance for Solar Power Applications," *Energies*, vol. 14, no. 20, Jan. 2021, Art. no. 6745, https://doi.org/10.3390/en14206745.

[4] K. Yeranee, Y. Rao, C. Xu, Y. Zhang, and X. Su, "Turbulent Flow Heat Transfer and Thermal Stress Improvement of Gas Turbine Blade Trailing Edge Cooling with Diamond-Type TPMS Structure," *Aerospace*, vol. 11, no. 1, Jan. 2024, Art. no. 37, https://doi.org/10.3390/aerospace11010037.

[5] K. Liu, "Heat transfer characteristics of triple-stage impingement designs and their application for industrial gas turbine combustor liner cooling," *International Journal of Heat and Mass Transfer*, vol. 172, Jun. 2021, Art. no. 121174, https://doi.org/10.1016/j.ijheatmasstransfer.2021.121174.

[6] W. Lian, Y. Jiang, H. Chen, Y. Li, and X. Liu, "Heat Transfer Characteristics of an Aeroengine Turbine Casing Based on CFD and the Surrogate Model," *Energies*, vol. 15, no. 18, Jan. 2022, Art. no. 6743, https://doi.org/10.3390/en15186743.

[7] K. D. C. Do, D. H. Chung, D. Q. Tran, C. T. Dinh, Q. H. Nguyen, and K. Y. Kim, "Numerical Investigation of Heat Transfer Characteristics of Pin-Fins with Roughed Endwalls in Gas Turbine Blade Internal Cooling Channels," *International Journal of Heat and Mass Transfer*, vol. 195, Oct. 2022, Art. no. 123125, https://doi.org/10.1016/j.ijheatmasstransfer.2022.123125.

[8] J. Ahn, "Large Eddy Simulation of Flow and Heat Transfer in a Ribbed Channel for the Internal Cooling Passage of a Gas Turbine Blade: A Review," *Energies*, vol. 16, no. 9, 2023, https://doi.org/10.3390/en16093656.

[9] T. S. Chowdhury, F. T. Mohsin, M. M. Tonni, M. N. H. Mita, and M. M. Ehsan, "A critical review on gas turbine cooling performance and failure analysis of turbine blades," *International Journal of Thermofluids*, vol. 18, May 2023, Art. no. 100329, https://doi.org/10.1016/j.ijft.2023.100329.

[10] K. Krishnaswamy and S. Sivan, "Improvement in thermal hydraulic performance by using continuous V and W-Shaped rib turbulators in gas turbine blade cooling application," *Case Studies in Thermal Engineering*, vol. 24, Apr. 2021, Art. no. 100857, https://doi.org/10.1016/j.csite.2021.100857.

[11] L. Xi, L. Xu, J. Gao, Z. Zhao, and Y. Li, "Numerical analysis and optimization on flow and heat transfer performance of a steam-cooled ribbed channel," *Case Studies in Thermal Engineering*, vol. 28, Dec. 2021, Art. no. 101442, https://doi.org/10.1016/j.csite.2021.101442.

[12] T. Xu, D. Shi, D. Zhang, and Y. Xie, "Flow and Heat Transfer Characteristics of the Turbine Blade Variable Cross-Section Internal Cooling Channel with Turning Vane," *Applied Sciences*, vol. 13, no. 3, 2023, https://doi.org/10.3390/app13031446.

[13] D. T. Vo, T. D. Mai, B. Kim, J. S. Jung, and J. Ryu, "Numerical investigation of crack initiation in high-pressure gas turbine blade subjected to thermal-fluid-mechanical low-cycle fatigue," *International Journal of Heat and Mass Transfer*, vol. 202, Mar. 2023, Art. no. 123748, https://doi.org/10.1016/j.ijheatmasstransfer.2022.123748.

[14] I. Guimarães, S. Baptista-Silva, M. Pintado, and A. L. Oliveira, "Polyphenols: A Promising Avenue in Therapeutic Solutions for Wound Care," *Applied Sciences*, vol. 11, no. 3, Jan. 2021, Art. no. 1230, https://doi.org/10.3390/app11031230.

[15] L. B. Inhestern, D. Peitsch, and G. Paniagua, "Flow irreversibility and heat transfer effects on turbine efficiency," *Applied Energy*, vol. 353, Jan. 2024, Art. no. 122077, https://doi.org/10.1016/j.apenergy.2023.122077.

[16] C. H. Hsu, J. L. Chen, S. C. Yuan, and K. Y. Kung, "CFD Simulations on the Rotor Dynamics of a Horizontal Axis Wind Turbine Activated from Stationary," *Applied Mechanics*, vol. 2, no. 1, pp. 147–158, Mar. 2021, https://doi.org/10.3390/applmech2010009.

[17] Y. Engineer, A. Rezk, and A. K. Hossain, "Energy analysis and optimization of a small-scale axial flow turbine for Organic Rankine Cycle application," *International Journal of Thermofluids*, vol. 12, Nov. 2021, Art. no. 100119, https://doi.org/10.1016/j.ijft.2021.100119.

[18] Z. Tao, Z. Guo, B. Yu, L. Song, and J. Li, "Aero-thermal optimization of a gas turbine blade endwall with non-axisymmetric contouring and purge flow," *International Journal of Heat and Mass Transfer*, vol. 178, Oct. 2021, Art. no. 121626, https://doi.org/10.1016/j.ijheatmasstransfer.2021.121626.

[19] H. Cui, L. Wang, X. Li, and J. Ren, "Data-Driven Conjugate Heat Transfer Analysis of a Gas Turbine Vane," *Processes*, vol. 10, no. 11, Nov. 2022, Art. no. 2335, https://doi.org/10.3390/pr10112335.

[20] A. Dong, P. Yan, X. Qian, W. Han, and Q. Wang, "Rotation Effect on Flow and Heat Transfer for High-Temperature Rotor Blade in a Heavy Gas Turbine," *Journal of Thermal Science*, vol. 30, no. 2, pp. 707–715, Mar. 2021, https://doi.org/10.1007/s11630-020-1319-x.

[21] N. Cao, X. Luo, and H. Tang, "A Bayesian model to solve a two-dimensional inverse heat transfer problem of gas turbine discs," *Applied Thermal Engineering*, vol. 214, Sep. 2022, Art. no. 118762, https://doi.org/10.1016/j.applthermaleng.2022.118762.

[22] Z. Zhao, L. Luo, D. Qiu, S. Wang, Z. Wang, and B. Sundén, "On the topology of vortex structures and heat transfer of a gas turbine blade internal tip with different arrangement of delta-winglet vortex generators," *International Journal of Thermal Sciences*, vol. 160, Feb. 2021, Art. no. 106676, https://doi.org/10.1016/j.ijthermalsci.2020.106676.

[23] Z. Zhao, L. Luo, D. Qiu, S. Wang, Z. Wang, and B. Sundén, "Influence of spacing of a delta-winglet vortex generator pair on the flow behavior and heat transfer at the internal tip of gas turbine blades," *International Journal of Thermal Sciences*, vol. 175, May 2022, Art. no. 107464, https://doi.org/10.1016/j.ijthermalsci.2022.107464.

[24] H. Abedi, C. Xisto, I. Jonsson, T. Grönstedt, and A. Rolt, "Preliminary Analysis of Compression System Integrated Heat Management Concepts Using LH2-Based Parametric Gas Turbine Model," *Aerospace*, vol. 9, no. 4, Apr. 2022, Art. no. 216, https://doi.org/10.3390/aerospace9040216.

[25] R. Zhang, P. Liu, X. Zhang, W. Xi, and J. Liu, "Recent Developments in the Aerodynamic Heat Transfer and Cooling Technology of Gas Turbines Endwalls," *Aerospace*, vol. 10, no. 8, Aug. 2023, Art. no. 702, https://doi.org/10.3390/aerospace10080702.

[26] J. Y. Jeong, W. Kim, J. S. Kwak, B. J. Lee, and J. T. Chung, "Effect of Mainstream Velocity on the Heat Transfer Coefficient of Gas Turbine Blade Tips," *Energies*, vol. 14, no. 23, Jan. 2021, Art. no. 7968, https://doi.org/10.3390/en14237968.

[27] Y. Cengel and J. Cimbala, *Fluid Mechanics Fundamentals and Applications*, 3rd ed. New York, NY, USA: McGraw Hill, 2013.

[28] D. G. Zill, *Advanced Engineering Mathematics*, 7th ed. Burlington, MA, USA: Jones & Bartlett Learning, 2020.

[29] P. Trojovský, M. Dehghani, and P. Hanuš, "Siberian Tiger Optimization: A New Bio-Inspired Metaheuristic Algorithm for Solving Engineering Optimization Problems," *IEEE Access*, vol. 10, pp. 132396–132431, 2022, https://doi.org/10.1109/ACCESS.2022.3229964.

[30] A. O. Griewank, "Generalized descent for global optimization," *Journal of Optimization Theory and Applications*, vol. 34, no. 1, pp. 11–39, May 1981, https://doi.org/10.1007/BF00933356.

[31] A. Alimoradi, "Heat transfer rates for shell and helically coiled finned tube heat exchangers." Mendeley Data, Dec. 05, 2016, https://doi.org/10.17632/m3mpy5xxnv.1.

[32] X. Gou, H. Zhang, G. Li, Y. Cao, and Q. Zhang, "Dynamic simulation of a gas turbine for heat recovery at varying load and environment conditions," *Applied Thermal Engineering*, vol. 195, Aug. 2021, Art. no. 117014, https://doi.org/10.1016/j.applthermaleng.2021.117014.

[33] S. Osipov, A. Rogalev, N. Rogalev, I. Shevchenko, and A. Vegera, "Asymmetric Method of Heat Transfer Intensification in Radial Channels of Gas Turbine Blades," *Inventions*, vol. 7, no. 4, Dec. 2022, Art. no. 117, https://doi.org/10.3390/inventions7040117.

[34] A. M. Alsaghir and J.-H. Bahk, "Performance Optimization and Exergy Analysis of Thermoelectric Heat Recovery System for Gas Turbine Power Plants," *Entropy*, vol. 25, no. 12, Dec. 2023, Art. no. 1583, https://doi.org/10.3390/e25121583.

[35] C. Yang, Y. Deng, N. Zhang, X. Zhang, G. He, and J. Bao, "Optimal structure design of supercritical CO2 power cycle for gas turbine waste heat recovery: A superstructure method," *Applied Thermal Engineering*, vol. 198, Nov. 2021, Art. no. 117515, https://doi.org/10.1016/j.applthermaleng.2021.117515.

[36] G. Dumitraşcu, M. Feidt, and Ş. Grigorean, "Finite Physical Dimensions Thermodynamics Analysis and Design of Closed Irreversible Cycles," *Energies*, vol. 14, no. 12, Jan. 2021, Art. no. 3416, https://doi.org/10.3390/en14123416.